First-principles study of electronic and optical properties of lead-free double perovskites Cs2NaBX6 (B = Sb, Bi; X = Cl, Br, I)

First-principles study of electronic and optical properties of lead-free double perovskites Cs_2NaBX_6 (B = Sb, Bi; X = Cl, Br, I)

Shuai Zhao[a, b, *], *Kumiko Yamamoto*[b], *Satoshi Iikubo*[b], *Shuzi Hayase*[b] *and Tingli Ma*[b *]

[a]School of Science, Chongqing University of Technology, Chongqing 400054, P. R. China

[b]Graduate School of Life Science and Systems Engineering, Kyushu Institute of Technology, Kitakyushu, Fukuoka, 808–0196, Japan

Corresponding email: zhaoshuai@cqut.edu.cn, tinglima@life.kyutech.ac.jp

ABSTRACT

Organolead halide perovskite has been regarded as the most promising light-harvesting material of next generation solar cells; however, the intrinsic instability and toxicity of lead are still the inevitable concern. The bismuth is ecofriendly and shows similar electronic properties with lead, which has attracted gradually interest in optoelectronic application. However, the valence state of bismuth is different with that of lead, eliminating the possibility of replacing lead by bismuth in organolead halide perovskites. To address this matter, one feasible strategy is to construct *B*-site double perovskites by the combination of half Bi^{3+} and half B^{+} cation. In this work, the lead-free halide double perovskites Cs_2Na*B*X_6 (*B* = Sb, Bi; *X* = Cl, Br, I) have been investigated by first-principles calculation. The electronic properties, optical absorption and thermodynamic stability of these compounds were investigated to ascertain the potential application of solar energy conversion. These results provide the theoretical support for the exploration of lead-free perovskite materials in the potential optoelectronic application.

Keywords: Lead-free Perovskites; Electronic Structure; DFT

1. INTRODUCTION

Organometal halide perovskite has revolutionized the landscape of the emerging photovoltaic (PV) technology with the impressive power conversion efficiency (PCE) [1,2]. To date, the highest certified PCE of the organolead halide perovskite solar cell has increased up to 22.1%, which is already comparable with the mature thin-film solar cells [3]. In addition to the high PCE, other merits, e.g., earth-abundant elements and low-cost fabrication method, allow the lead halide perovskite to be the most promising light-harvesting material for the next generation solar cells [4–6]. However, the low chemical stability under ambient air and the environmental risk of lead leaching are still the inescapable concern in the widespread application [7,8]. There is therefore an urgent to explore stable lead-free materials for perovskite solar cells.

Replacing all or part of lead by tin in the organolead halide perovskite has been investigated to eliminate or minimize the contamination risk [9–12]. The solar cell based on the perovskite $CH_3NH_3SnI_3$ exhibited a notable PCE of 6% [13]. Although tin is nontoxic, tin-based halide perovskites suffer from the oxidization of Sn^{2+} to Sn^{4+} states, which will impair the performance of devices [14]. Currently, nontoxic bismuth-based materials are gradually attracting attention in the optoelectronic application [15–17]. As two adjacent elements on the periodic table, bismuth and lead show some similar properties, e.g., the same electron configuration $5d^{10}6s^26p^0$ for their stable cations. A series of bismuth halide has been studied for the optoelectronic application, such as BiI_3, Bi*X* (*X* = O, S and Se) and $A_3Bi_2I_9$ (*A* = K, Rb, Cs, CH_3NH_3 or NH_4) [18–20]. These materials, however, are commonly low-dimensional compounds, which are different from the methylammonium (MA) lead halide perovskite with corner-sharing octahedral structure. Given the different valence, it is impracticable to directly substitute the lead by bismuth meanwhile satisfy the total charge neutrality. To solve this matter,

a feasible method is to form the *B*-site double perovskite $A_2B'B''X_6$, i.e., substituting the Pb^{2+} by half Bi^{3+} with half monovalent cation. Some noble metals (e.g., Cu and Ag) were employed as the substituted monovalent element, which has demonstrated to be an efficient strategy to explore novel lead-free perovskite materials [21–29].

The bismuth-based double perovskite $Cs_2NaBiCl_6$ was synthesized in the 1970s focusing on the study of the ferroelectric phase transition property [30,31]. In consideration of the ionic radius, the Na^+ (116 pm) is closer to Bi^{3+} (117 pm) than Ag^+ (129 pm) [32]. Similar to the lead halide perovskites, the band gap of $Cs_2NaBiCl_6$ is too large to be used as the visible-light absorber. To the best of our knowledge, substitution of *X*-site Cl by Br or I is still not reported for Na-based double perovskites by experiments. Motivated by this, we investigated a series of double perovskites Cs_2NaBX_6 (*B* = Sb, Bi; *X* = Cl, Br, I) by using the first-principles calculation based on density functional theory (DFT). The electronic properties, optical absorption and thermodynamic stability were calculated for these compounds. These results can be useful guide of the development of lead-free double perovskite materials.

2. COMPUTATIONAL METHODS

The DFT calculations were implemented in the Quantum ESPRESSO software package with the plane-wave pseudopotential approach [33,34]. The exchange correlation effects were described by the generalized gradient approximation (GGA) with the Perdew-Burke-Ernzerhof (PBE) functional [35]. The ultra-soft pseudopotentials were considered for the election-ion interactions. A plane wave cutoff of 40 Ry was adopted for the expansion of the wave functions, and the 4 x 4 x 4 Monkhorst-Pack *k*-mesh grid was employed for the ground state calculations [36]. All the

compounds were fully relaxed until the cell stresses were less than 10^{-4} Ry/bohr^3 and the residual forces were less than 10^{-3} Ry/bohr on each atomic site. Considering the relativistic effects of heavier metals, we employed the fully relativistic ultrasoft pseudopotentials with spin-orbit coupling (SOC) for the calculation of electronic properties. It is a well-known fact that the DFT method usually underestimates the band gap of semiconductors. To overcome the underestimation, we employed the Heyd–Scuseria–Ernzerhof hybrid functional (HSE06) to calculate the band gap of iodide perovskites. The HSE06 calculations were carried out by Vienna *Ab initio* Simulation Package (VASP) with the projector-augmented wave method [37]. To study the optical properties, we calculated the frequency dependent complex dielectric function $\varepsilon(\omega) = \varepsilon_r(\omega) + i\cdot\varepsilon_i(\omega)$ with a denser *k*-mesh grid. The absorption coefficient $\alpha(\omega)$ is computed by means of the formula:

$$\alpha(\omega) = \frac{4\pi}{\lambda}\sqrt{\frac{-\varepsilon_r(\omega) + \sqrt{\varepsilon_r^2(\omega) + \varepsilon_i^2(\omega)}}{2}} \quad (1)$$

where λ and ω are the wavelength and frequency of the incident light, respectively.

3. RESULTS AND DISCUSSION

Starting from the experimental parameters of $Cs_2NaBiCl_6$ (*Fm*3*m*, 10.839Å, face-centered cubic) [30,31,38], we fully optimized the lattice parameters for all these double perovskites. The atomic structure is shown in **Fig. 1** and the relaxed lattice parameters are presented in **Table 1**. Compared with the measured value of $Cs_2NaBiCl_6$, we can see that the PBE method exhibits excellent prediction ability for lattice parameters. The optimized lattice constants of these materials show two tendencies: 1) lattice constants increase with the order of *X* = Cl, Br and I; 2)

Sb-based double perovskites have smaller lattice constants compared with the corresponding Bi-based compounds. These results can be ascribed to the different ionic radii of the *B*- and *X*-sites ions. The ionic radius becomes longer with the increase of the atomic number, leading to the increase of lattice constant. Moreover, the increase of Na-*X* bond-lengths was also observed among these materials with the lattice expansion.

The electronic structures of these double perovskites were calculated by scalar and fully relativistic PBE pseudopotentials. The predicted band gaps are presented in **Table 2**. We can see that the electronic band gaps of these perovskites exhibit a decrease tendency in order of *X* = Cl, Br, and I. With the treatment of SOC effects, the electronic band gaps were reduced significantly. The band dispersions are illustrated in **Fig. 2**. We can see that these double perovskites were predicted to be of indirect gap. The conduction band minimum (CBM) was predicted to appear at the *L* (π/a, π/a, π/a) point in the Brillouin zone for all compounds. The valence band maximum (VBM) exhibits several features. For Cs_2NaSbI_6, the VBM was found at the *X* (2π/a, 0, 0) point. For Cs_2NaBiI_6, the VBM was predicted at the Γ (0, 0, 0) point. For other compounds, the VBM are all at *W* (2π/a, π/a, 0) point. When taking into account the SOC effects, these materials show different electronic properties compared with PBE results. The upper valence bands exhibit the similar dispersions for both PBE and PBE+SOC calculations. But for lower conduction bands, the obvious split off arises from the SOC effect. The spin-orbit split off results into the reduction of electronic band gaps. The underestimation of band gap by employing SOC effects can be also found in the organometal halide perovskite or other bismuth halide compounds [11,17,23]. For instance, the band gap of the perovskite $CH_3NH_3PbI_3$ was predicted to be 0.60 eV by SOC-DFT, which is significantly lower than the experimental value [11]. However, taking into account the SOC effects doesn't affect the physical tendency of band gaps and is critical to understand the

electronic properties of these materials [39]. For Cs_2NaBiI_6, apart from the reduction of indirect band gap, the spin-orbit split off leads to the decrease of the CBM at the Γ point, resulting into a direct band gap of 1.71 eV at Γ point, which is slightly larger than the indirect value 1.68 eV. A better calculation of the band gap can be reached by preforming the HSE06 or GW self-energy corrections. However, accounting both SOC and these correction methods would need huge computational resources. In these compounds, iodide perovskites Cs_2NaSbI_6 and Cs_2NaBiI_6 exhibit the potential in the application of solar cells due to optimal gap values at PBE level. To further evaluate the potential application in solar cells, we calculated the band gaps of these two iodide compounds by HSE06 method with SOC effects. The predicted band gaps at HSE06+SOC level are 2.06 and 2.43 eV for Cs_2NaSbI_6 and Cs_2NaBiI_6, respectively. Despite the fact that band gaps decrease with the order of Cl, Br, I, iodide double perovskites have still large band gap, limiting the efficient visible-light harvesting.

A further understanding of the electronic properties can be investigated from the partial density of states (PDOS). For these double perovskites, upper valence bands are dominated by *p*-state electrons of halogen anions with a small contribution from the *s*-orbital electrons of pnictogens. This reveals the stereo-chemical lone pair *s*-orbital electrons of Sb and Bi in these materials. The lower conduction bands are predominantly contributed by the interaction of *p*-orbital electrons between pnictogens and halogens. Therefore, the conduction bands undergo an obvious spin-orbit split off in consideration of the SOC effect. Although the *B*-site Na plays an important role in the formation of the double perovskite structure, the Na *s*-orbital electrons are negligible at the upper valence and lower conduction bands. Moreover, the *A*-site Cs *s* electrons only become dominant at higher conduction bands. These PDOS results reveal the distribution of photo-generated electron-hole pairs in these materials. The *s*-states of pnictogens and *p*-states of

halogens are involved in the formation of holes, while their *p*-states contribute to the formation of electrons.

The photocarriers effective masses (m^*_e and m^*_h) can be calculated on basis of the parabolic approximation of the band dispersion at CBM and VBM according to the following relation [40]:

$$\frac{1}{m^*} = \frac{1}{\hbar^2} \cdot \frac{\partial^2 E(k)}{\partial k^2} \quad (2)$$

where the $E(k)$ is the eigenvalue and k is the wavevector. The estimated effective masses are listed in **Table 2** for these double perovskites. It can be seen that the photocarriers effective masses show the decreasing trend in order of Cl, Br and I among these double perovskites, similar to the tendency of band gaps. This indicates that substitution of *X*-site anions is conducive not only to the reduction of band gap but also to the enhancement of photocarriers mobility. The estimated effective masses of electrons are small, indicating the high mobility of photon-generated electrons in these double perovskites. While effective masses of holes are relatively larger due to the flat valence band dispersions, suggesting the inferior mobility of holes. In the $MAPbI_3$ perovskite, the mobility of holes at the VBM is usually superior to that of electrons, and this outstanding mobility of holes has been regarded as a critical feature for the high performance of perovskite solar cells [41]. However, the mobility of photo-generated holes in these double perovskites is interior to that of electrons, suggesting that both the band gap and carriers mobility are required to be tuned in order to obtain a high performance of solar cells using these double perovskites.

To investigate the visible-light harvesting capacity, we calculated the absorption coefficiency of these double perovskites as shown in **Fig. 3**. As the absorption threshold is

inversely proportional to the band gap, the double perovskites with narrow band gaps are expected to possess the broad absorption in visible range. Among these double perovskites, Cs_2NaSbI_6, Cs_2NaBiI_6 and $Cs_2NaSbBr_6$ exhibit efficient absorption in the visible range. As shown in PDOS results, the absorption of these double perovskites is a *p-p* transition from valence to conduction bands, similar to the lead halide perovskites. However, the band gaps of these compounds are indirect, which impacts the absorption magnitude. This can be evidenced by the comparison with $CsPbI_3$ as shown in **Fig. 3**, which is predicted to be a direct band gap semiconductor. The $Cs_2NaBiCl_6$ is the only double perovskite synthesized by experiment, but the absorption range is lower than 320 nm of wavelength. Although it is not suitable for solar cells, the $Cs_2NaBiCl_6$ can be explored in the application of ultraviolet sensors or detectors.

To assess the stability of these double perovskites, we calculated the energies of these compounds to determine the thermodynamic stability based on the chemical reaction [42]:

$$2\cdot Cs_2NaBX_6 \leftrightarrow Cs_3B_2X_9 + 2\cdot NaX + CsX \quad (3)$$

and the formation enthalpy ΔH can be calculated by [43]:

$$\Delta H = 2\cdot H(Cs_2NaBX_6) - [H(Cs_3B_2X_9) + 2\cdot H(NaX) + H(CsX)] \quad (4)$$

considering the solid phase of these materials at the atmospheric pressure, we applied the approximation of $\Delta H \approx \Delta E$ for these calculations. The calculated formation enthalpies for these double perovskites are listed in **Table 3**. We can see that the chloride perovskites have the negative formation enthalpy, indicating that the phase decomposition is endothermic. Thus, the double perovskite phase of these chlorides is thermodynamic stable. While in the bromide and iodide perovskites, the formation enthalpies are predicted to be positive, suggesting that the phase decomposition of these double perovskites is spontaneous. The calculated formation

enthalpies for Cs_2NaSbI_6 and Cs_2NaBiI_6 are similar to that of Cs_2AgBiI_6 (0.41 eV per formula) in previous study [42]. Although the iodide perovskites have the smaller band gaps, they suffer from the thermodynamic instability. However, a recent study reported that the $(CH_3NH_3)_2AgBiI_6$ powder has been synthesized by solid-state reaction, and shows stability in the air [24]. This suggests that the bromide and iodide perovskites are still possible stable under certain condition that the kinetic barrier would hinder the decomposition reaction [43].

4. CONCLUSIONS

In summary, we investigated the electronic properties of double perovskites $Cs_2Na\mathit{BX}_6$ (*B* = Sb, Bi; *X* = Cl, Br, I) by using the first-principles calculation with focus on the potential optoelectronic application. All these double perovskites were predicted to possess indirect band gap. The Sb-based double perovskite has smaller band gap than the corresponding Bi-based compound. For the perovskites with the same *B*-site cations, the gap values decrease with the order of Cl, Br and I. These double perovskites have small efficient masses for photo-generated electrons at CBM but large efficient masses for holes due to the flat band dispersion at VBM. The absorption coefficients reveal that only Cs_2NaSbI_6, Cs_2NaBiI_6 and $Cs_2NaSbBr_6$ could efficiently absorb the photon in the visible-light range. The formation enthalpy results revealed that only the chloride compounds have stable double perovskite phase among these materials. These results provide theoretical suggestions for the development of novel lead-free double perovskite materials for opto-electronic applications.

ACKNOWLEDGEMENTS

This work was supported by Grant-in-Aid for Scientific Research of (KAKENHI) program, Japan (C, Grant Number 15K05597).

REFERENCES

[1] A. Kojima, K. Teshima, Y. Shirai, T. Miyasaka, Organometal halide perovskites as visible-light sensitizers for photovoltaic cells, J. Am. Chem. Soc. 131 (2009) 6050–6051. doi:10.1021/ja809598r.

[2] M. Saliba, S. Orlandi, T. Matsui, S. Aghazada, M. Cavazzini, J.P. Correa-Baena, P. Gao, R. Scopelliti, E. Mosconi, K.H. Dahmen, F. De Angelis, A. Abate, A. Hagfeldt, G. Pozzi, M. Graetzel, M.K. Nazeeruddin, A molecularly engineered hole-transporting material for efficient perovskite solar cells, Nat. Energy. 1 (2016) 15017. doi:10.1038/nenergy.2015.17.

[3] W.S. Yang, B.-W. Park, E.H. Jung, N.J. Jeon, Y.C. Kim, D.U. Lee, S.S. Shin, J. Seo, E.K. Kim, J.H. Noh, S. Il Seok, Iodide management in formamidinium-lead-halide–based perovskite layers for efficient solar cells, Science (80-.). 356 (2017) 1376–1379. doi:10.1126/science.aan2301.

[4] M. Liu, M.B. Johnston, H.J. Snaith, Efficient planar heterojunction perovskite solar cells by vapour deposition, Nature. 501 (2013) 395–398. doi:10.1038/nature12509.

[5] J. Burschka, N. Pellet, S.-J. Moon, R. Humphry-Baker, P. Gao, M.K. Nazeeruddin, M. Grätzel, Sequential deposition as a route to high-performance perovskite-sensitized solar cells, Nature. (2013). doi:10.1038/nature12340.

[6] T.M. Brenner, D.A. Egger, L. Kronik, G. Hodes, D. Cahen, Hybrid organic—inorganic perovskites: low-cost semiconductors with intriguing charge-transport properties, Nat. Rev. Mater. 1 (2016) 15007. doi:10.1038/natrevmats.2015.7.

[7] L. Serrano-Lujan, N. Espinosa, T.T. Larsen-Olsen, J. Abad, A. Urbina, F.C. Krebs, Tin- and lead-based perovskite solar cells under scrutiny: An environmental perspective, Adv. Energy Mater. 5 (2015) 1501119. doi:10.1002/aenm.201501119.

[8] A. Babayigit, A. Ethirajan, M. Muller, B. Conings, Toxicity of organometal halide perovskite solar cells, Nat. Mater. 15 (2016) 247–251. doi:10.1038/nmat4572.

[9] Y. Ogomi, A. Morita, S. Tsukamoto, T. Saitho, N. Fujikawa, Q. Shen, T. Toyoda, K. Yoshino, S.S. Pandey, T. Ma, S. Hayase, CH3NH3SnxPb(1–x)I3 Perovskite Solar Cells Covering up to 1060 nm, J. Phys. Chem. Lett. 5 (2014) 1004–1011. doi:10.1021/jz5002117.

[10] F. Hao, C.C. Stoumpos, D.H. Cao, R.P.H. Chang, M.G. Kanatzidis, Lead-free solid-state organic–inorganic halide perovskite solar cells, Nat. Photonics. 8 (2014) 489–494. doi:10.1038/nphoton.2014.82.

[11] P. Umari, E. Mosconi, F. De Angelis, Relativistic GW calculations on CH3NH3PbI3 and CH3NH3SnI3 perovskites for solar cell applications., Sci. Rep. 4 (2014) 4467. doi:10.1038/srep04467.

[12] C. Bernal, K. Yang, First-Principles Hybrid Functional Study of the Organic–Inorganic Perovskites CH3NH3SnBr3 and CH3NH3SnI3, J. Phys. Chem. C. 118 (2014) 24383–24388.

[13] N.K. Noel, S.D. Stranks, A. Abate, C. Wehrenfennig, S. Guarnera, A.-A. Haghighirad, A. Sadhanala, G.E. Eperon, S.K. Pathak, M.B. Johnston, A. Petrozza, L.M. Herz, H.J. Snaith, Lead-free organic–inorganic tin halide perovskites for photovoltaic applications, Energy Environ. Sci. 7 (2014) 3061–3068. doi:10.1039/C4EE01076K.

[14] E.S. Parrott, R.L. Milot, T. Stergiopoulos, H.J. Snaith, M.B. Johnston, L.M. Herz, Effect of Structural Phase Transition on Charge-Carrier Lifetimes and Defects in CH3NH3SnI3 Perovskite, J. Phys. Chem. Lett. 7 (2016) 1321–1326. doi:10.1021/acs.jpclett.6b00322.

[15] R.L.Z. Hoye, R.E. Brandt, A. Osherov, V. Stevanovic, S.D. Stranks, M.W.B. Wilson, H. Kim, A.J. Akey, J.D. Perkins, R.C. Kurchin, J.R. Poindexter, E.N. Wang, M.G. Bawendi, V. Bulovic, T. Buonassisi, Methylammonium Bismuth Iodide as a Lead-Free, Stable Hybrid Organic-Inorganic Solar Absorber, Chem. - A Eur. J. 22 (2016) 2605–2610. doi:10.1002/chem.201505055.

[16] F. Wei, Z. Deng, S. Sun, F. Xie, G. Kieslich, D.M. Evans, M.A. Carpenter, P.D. Bristowe, A.K. Cheetham, The synthesis, structure and electronic properties of a lead-free hybrid inorganic–organic double perovskite (MA) 2 KBiCl 6 (MA = methylammonium), Mater. Horiz. 3 (2016) 328–332. doi:10.1039/C6MH00053C.

[17] A.M. Ganose, M. Cuff, K.T. Butler, A. Walsh, D.O. Scanlon, Interplay of Orbital and Relativistic Effects in Bismuth Oxyhalides: BiOF, BiOCl, BiOBr, and BiOI, Chem. Mater. 28 (2016) 1980–1984. doi:10.1021/acs.chemmater.6b00349.

[18] R.E. Brandt, R.C. Kurchin, R.L.Z. Hoye, J.R. Poindexter, M.W.B. Wilson, S. Sulekar, F. Lenahan, P.X.T. Yen, V. Stevanović, J.C. Nino, M.G. Bawendi, T. Buonassisi, Investigation of Bismuth Triiodide (BiI3) for Photovoltaic Applications, J. Phys. Chem. Lett. 6 (2015) 4297–4302. doi:10.1021/acs.jpclett.5b02022.

[19] A.J. Lehner, D.H. Fabini, H.A. Evans, C.A. Hébert, S.R. Smock, J. Hu, H. Wang, J.W. Zwanziger, M.L. Chabinyc, R. Seshadri, Crystal and Electronic Structures of Complex Bismuth Iodides A3Bi2I9 (A = K, Rb, Cs) Related to Perovskite: Aiding the Rational Design of Photovoltaics, Chem. Mater. 27 (2015) 7137–7148. doi:10.1021/acs.chemmater.5b03147.

[20] S. Sun, S. Tominaka, J.H. Lee, F. Xie, P.D. Bristowe, A.K. Cheetham, Synthesis, crystal structure, and properties of a perovskite-related bismuth phase, (NH4)3Bi2I9, APL Mater. 4 (2016). doi:10.1063/1.4943680.

[21] E.T. McClure, M.R. Ball, W. Windl, P.M. Woodward, Cs2AgBiX6 (X = Br, Cl): New Visible Light Absorbing, Lead-Free Halide Perovskite Semiconductors, Chem. Mater. 28 (2016) 1348–1354. doi:10.1021/acs.chemmater.5b04231.

[22] A.H. Slavney, T. Hu, A.M. Lindenberg, H.I. Karunadasa, A Bismuth-Halide Double Perovskite with Long Carrier Recombination Lifetime for Photovoltaic Applications, J. Am. Chem. Soc. 138 (2016) 2138–2141. doi:10.1021/jacs.5b13294.

[23] G. Volonakis, M.R. Filip, A.A. Haghighirad, N. Sakai, B. Wenger, H.J. Snaith, F. Giustino, Lead-Free Halide Double Perovskites via Heterovalent Substitution of Noble Metals, J. Phys. Chem. Lett. 7 (2016) 1254–1259. doi:10.1021/acs.jpclett.6b00376.

[24] P. Cheng, T. Wu, Y. Li, L. Jiang, W.-Q. Deng, K. Han, Combining Theory and Experiment in the Design of a Lead-Free (CH3NH3)2AgBiI6 Double Perovskite, New J. Chem. (2017). doi:10.1039/C7NJ02365K.

[25] M.R. Filip, S. Hillman, A.A. Haghighirad, H.J. Snaith, F. Giustino, Band Gaps of the Lead-Free Halide Double Perovskites Cs2BiAgCl6 and Cs2BiAgBr6 from Theory and Experiment, J. Phys. Chem. Lett. 7 (2016) 2579–2585. doi:10.1021/acs.jpclett.6b01041.

[26] E. Greul, M.L. Petrus, A. Binek, P. Docampo, T. Bein, Highly stable, phase pure Cs2AgBiBr6 double perovskite thin films for optoelectronic applications, J. Mater. Chem. A. 0 (2017) 1–10. doi:10.1039/C7TA06816F.

[27] Z. Xiao, W. Meng, J. Wang, D.B. Mitzi, Y. Yan, Searching for promising new perovskite-based photovoltaic absorbers: the importance of electronic dimensionality, Mater. Horiz. 4 (2017) 206–216. doi:10.1039/C6MH00519E.

[28] G. Volonakis, A.A. Haghighirad, R.L. Milot, W.H. Sio, M.R. Filip, B. Wenger, M.B. Johnston, L.M. Herz, H.J. Snaith, F. Giustino, Cs2InAgCl6: A New Lead-Free Halide Double Perovskite with Direct Band Gap, J. Phys. Chem. Lett. 8 (2017) 772–778. doi:10.1021/acs.jpclett.6b02682.

[29] G. Volonakis, A.A. Haghighirad, H.J. Snaith, F. Giustino, Route to Stable Lead-Free Double Perovskites with the Electronic Structure of CH3NH3PbI3: A Case for Mixed-Cation [Cs/CH3NH3/CH(NH2)2]2InBiBr6, J. Phys. Chem. Lett. 8 (2017) 3917–3924. doi:10.1021/acs.jpclett.7b01584.

[30] L.R. Morrs, W.R. Robinson, Crystal structure of Cs2NaBiCl6, Acta Crystallogr. Sect. B. B28 (1972) 653–654. doi:10.1107/S0567740872002948.

[31] L.R. Morss, M. Siegal, L. Stenger, N. Edelstein, Preparation of cubic chloro complex compounds of trivalent metals: Cs2NaMCl6, Inorg. Chem. 9 (1970) 1771–1775. doi:10.1021/ic50089a034.

[32] R.D. Shannon, Revised effective ionic radii and systematic studies of interatomic distances in halides and chalcogenides, Acta Crystallogr. Sect. A. 32 (1976) 751–767. doi:10.1107/S0567739476001551.

[33] P.E. Blöchl, Projector augmented-wave method, Phys. Rev. B - Condens. Matter Mater. Phys. 50 (1994) 17953–17979. doi:10.1103/PhysRevB.50.17953.

[34] P. Giannozzi, S. Baroni, N. Bonini, M. Calandra, R. Car, C. Cavazzoni, D. Ceresoli, G.L. Chiarotti, M. Cococcioni, I. Dabo, A. Dal Corso, S. de Gironcoli, S. Fabris, G. Fratesi, R. Gebauer, U. Gerstmann, C. Gougoussis, A. Kokalj, M. Lazzeri, L. Martin-Samos, N. Marzari, F. Mauri, R. Mazzarello, S. Paolini, A. Pasquarello, L. Paulatto, C. Sbraccia, S. Scandolo, G. Sclauzero, A.P. Seitsonen, A. Smogunov, P. Umari, R.M. Wentzcovitch, QUANTUM ESPRESSO: a modular and open-source software project for quantum simulations of materials, J. Phys. Condens. Matter. 21 (2009) 395502. doi:10.1088/0953-8984/21/39/395502.

[35] J.P. Perdew, K. Burke, M. Ernzerhof, Generalized Gradient Approximation Made Simple, Phys. Rev. Lett. 77 (1996) 3865–3868. doi:10.1103/PhysRevLett.77.3865.

[36] J.D. Pack, H.J. Monkhorst, "Special points for Brillouin-zone integrations"—a reply, Phys. Rev. B - Condens. Matter Mater. Phys. 16 (1977) 1748–1749. doi:10.1103/PhysRevB.16.1748.

[37] G. Kresse, J. Furthmüller, Efficient iterative schemes for ab initio total-energy calculations using a plane-wave basis set, Phys. Rev. B - Condens. Matter Mater. Phys. 54 (1996) 11169–11186. doi:10.1103/PhysRevB.54.11169.

[38] G. Meyer, S. ‐ J Hwu, J.D. Corbett, Low ‐ temperature crystal growth of Cs2LiLuCl6 ‐ II and Cs2KScCl6 under reducing conditions and their structural refinement, ZAAC ‐ J. Inorg. Gen. Chem. 535 (1986) 208–212. doi:10.1002/zaac.19865350423.

[39] A. Amat, E. Mosconi, E. Ronca, C. Quarti, P. Umari, M.K. Nazeeruddin, M. Grätzel, F. De Angelis, Cation-induced band-gap tuning in organohalide perovskites: Interplay of spin-orbit coupling and octahedra tilting, Nano Lett. 14 (2014) 3608–3616. doi:10.1021/nl5012992.

[40] G. Giorgi, J.I. Fujisawa, H. Segawa, K. Yamashita, Small photocarrier effective masses featuring ambipolar transport in methylammonium lead iodide perovskite: A density functional analysis, J. Phys. Chem. Lett. 4 (2013) 4213–4216. doi:10.1021/jz4023865.

[41] W.J. Yin, T. Shi, Y. Yan, Unique properties of halide perovskites as possible origins of the superior solar cell performance, Adv. Mater. 26 (2014) 4653–4658. doi:10.1002/adma.201306281.

[42] C.N. Savory, A. Walsh, D.O. Scanlon, Can Pb-Free Halide Double Perovskites Support High-Efficiency Solar Cells?, ACS Energy Lett. 1 (2016) 949–955. doi:10.1021/acsenergylett.6b00471.

[43] U.-G. Jong, C.-J. Yu, Y.-M. Jang, G.-C. Ri, S.-N. Hong, Y.-H. Pae, Revealing the stability and efficiency enhancement in mixed halide perovskites MAPb(I1–xClx)3 with ab initio calculations, J. Power Sources. 350 (2017) 65–72. doi:10.1016/j.jpowsour.2017.03.038.

Table 1. Optimized lattice constant a and Na-X bond-length $d_{Na\text{-}X}$ for Cs_2NaBX_6 (B = Sb and Bi; X = Cl, Br and I).

	a (Å)	$d_{Na\text{-}X}$ (Å)
$Cs_2NaSbCl_6$	10.652	2.692
$Cs_2NaSbBr_6$	11.223	2.829
Cs_2NaSbI_6	12.056	3.042
$Cs_2NaBiCl_6$	10.837 (10.839[a])	2.717 (2.759[a])
$Cs_2NaBiBr_6$	11.364	2.841
Cs_2NaBiI_6	12.199	3.054

[a]Reference [30]

Table 2. Calculated band gap E_g and photocarriers effective mass m^* for Cs_2NaBX_6 (B = Sb and Bi; X = Cl, Br and I).

	E_g (eV)			effective mass (m^*/m_0)	
	PBE	PBE+SOC	HSE06+SOC	m^*_h	m^*_e
$Cs_2NaSbCl_6$	3.13	2.96	-	1.62	0.56
$Cs_2NaSbBr_6$	2.54	2.37	-	1.09	0.39
Cs_2NaSbI_6	1.90	1.65	2.06	0.68	0.27
$Cs_2NaBiCl_6$	3.73	2.86	-	1.87	0.58
$Cs_2NaBiBr_6$	3.07	2.40	-	1.29	0.41
Cs_2NaBiI_6	2.23	1.68	2.43	0.58	0.28

Table 3. Calculated formation enthalpy ΔH for these double perovskites.

	$Cs_2NaSbCl_6$	$Cs_2NaSbBr_6$	Cs_2NaSbI_6	$Cs_2NaBiCl_6$	$Cs_2NaBiBr_6$	Cs_2NaBiI_6
ΔH (eV)	-0.19	0.11	0.49	-0.43	0.01	0.40

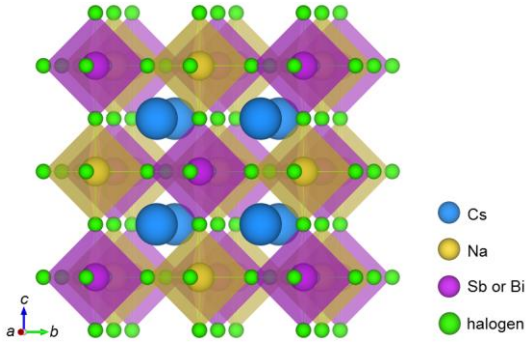

Fig. 1. Crystal schematic diagrams of these double perovskites Cs_2NaBX_6 (B = Sb, Bi; X = Cl, Br, I).

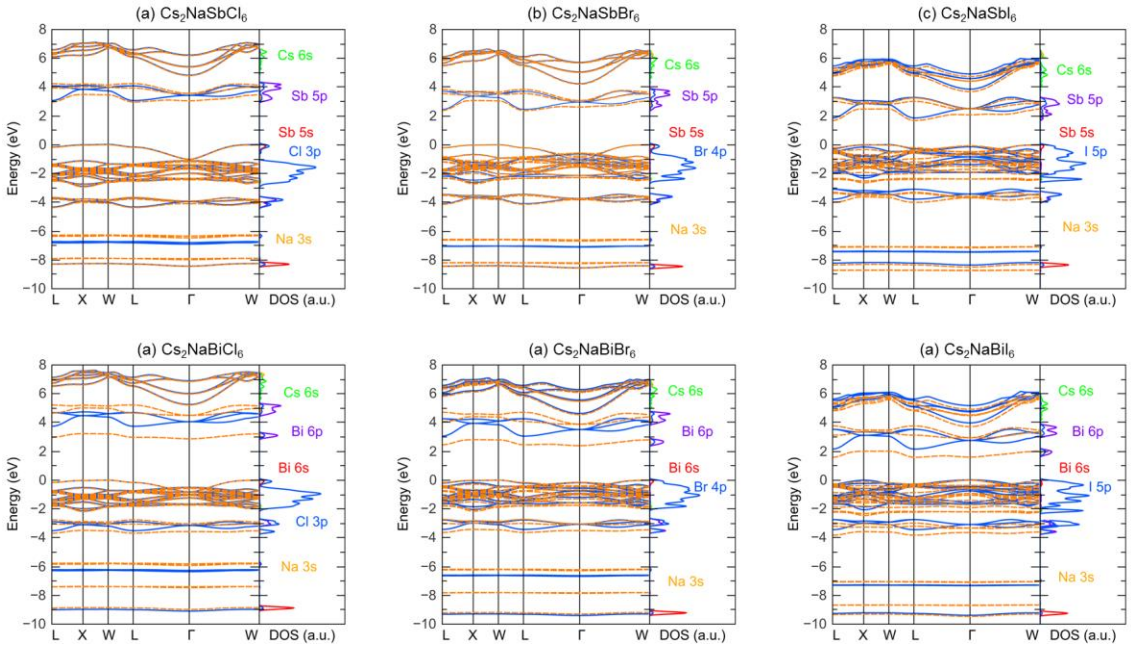

Fig. 2. Scalar relativistic (blue solid lines) and fully relativistic (orange dashed lines) band structures and fully relativistic partial density of states for these double perovskites. The highest occupied state is set to 0 eV.

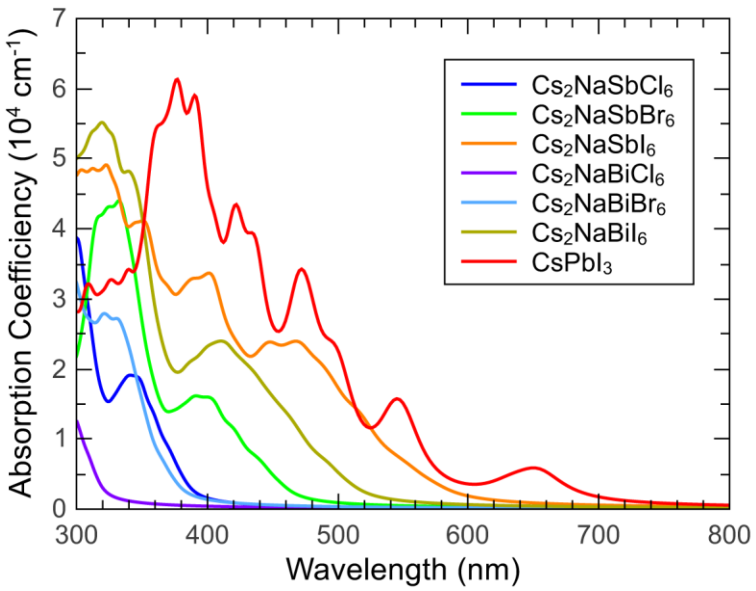

Fig. 3. Calculated optical absorption spectrum for these double perovskites $Cs_2Na\mathit{BX}_6$ (*B* = Sb, Bi; *X* = Cl, Br, I) compared with $CsPbI_3$.